AIAA SciTech Forum
January 3-7, 2022, San Diego, CA & Virtual
AIAA SCITECH 2022 Forum

10.2514/6.2022-1155

Reflections On Using Potential Flow Codes to Design High-Lift Systems

Gabino Martinez-Rodriguez [1]
and
Timothy T. Takahashi[2]

Arizona State University, Tempe, AZ, USA

This study showcases how low-order computational aerodynamic techniques can support conceptual as well as preliminary design of aircraft. Here, a Stratford Separation Criteria post processor was developed and coupled with a legacy Panel Method Potential Flow Code, VORLAX. After validation of this implementation with experimental data in 2D, we demonstrate the ways the flow over an airfoil, especially the incipient flow separation, is affected with the addition of high lift devices on the leading and trailing edge. After assessing the 2D case, we demonstrate the many ways how flow over a practical wing differs from a classical 2D analysis. Trade studies show how a finite wingspan, leading edge sweep, planform "Yehudi's" and planform taper impact the flow over a flapped wing, radically altering incipient flow separation conditions from the 2D analysis.

I. Introduction

ENGINEERS, historically, have depended upon extensive experimentation to design and develop commercial transport aircraft flap systems. Whether these studies are performed in a wind tunnel or during flight test, the number and extent of high-lift system variations that can be tested are limited by time and cost. With technology advancements, it is more common to analyze the complex flow around high-lift systems using detailed computational fluid dynamics (CFD) but, CFD has limitations due to its complex setup time and computing infrastructure. While an empirical approach can be taken to "spec-out" a high-lift system, the insight gained from such a process is limited.

This paper provides further evidence to support the use of Potential Flow panel-method codes (rather than volume-grid CFD methods) to design multi-element high-lift systems. We augment the output of a potential flow code with other methods derived from classical aerodynamic literature, specifically implementing Stratford's Method to predict incipient flow separation. Here, we apply these tools to 2D airfoil and 3D finite-swept-wing configurations and show the sorts of insight we develop using this method to screen many candidate wings. We found that this approach greatly speeds up the trade-study and design process because it keeps the engineer "in-the-loop" with near real-time feedback.

II. Motivation and History of High-lift Systems

Airlines push airframe suppliers to develop new aircraft with ever lower fuel consumption. Flight efficiency can be significantly increased by improving cruise aerodynamics. Since cruise comprises most of the flight, the importance of the cruise wing design cannot be underestimated. However, takeoff and landing are equally critical to mission success; aircraft must be able to take off and land within acceptable runway length limits. Unfortunately, many design features that increase cruise speed and cruise efficiency are unfavorable for low-speed, high-lift performance. With a well implemented rapid screening tool, the engineer can avoid design features on the cruise wing which hinder its performance with flaps and slats deployed.

[1] M.S. Candidate, Aerospace and Mechanical Engineering, School for Engineering of Matter, Transport & Energy, P.O. Box 876106, Tempe, AZ, 85281, Student Member AIAA
[2] Professor of Practice, Aerospace and Mechanical Engineering, School for Engineering of Matter, Transport & Energy, P.O. Box 876106, Tempe, AZ, 85281, Associate Fellow AIAA

A. Flapped Airfoils

The idea of increasing the lift generated by a wing by adding an additional device is by no means a new concept in aerodynamics. Early versions of flaps can be found in "Experiments on an Aerofoil Having a Hinged Rear Portion" published in 1914 by the British Aeronautical Research Council; see FIGURE 1. [1] Even before this, the 1910 LeBlon monoplane used a form of variable camber wing.[2] The discovery of slotted devices quickly followed; Sir Frederick Handley Page presented his work on slotted airfoils in 1921; [3] he proposed that adding more elements to an airfoil increased the lift, and even gave a worked example with an 8-element airfoil. The most important development was made by Harlan Fowler in 1931 [4]; his namesake flap deflected and extended forming a gap between the two-elements. This is the basis for flaps on most modern transport aircraft.

FIGURE 1 – RAF Airfoil from 1914 [1]

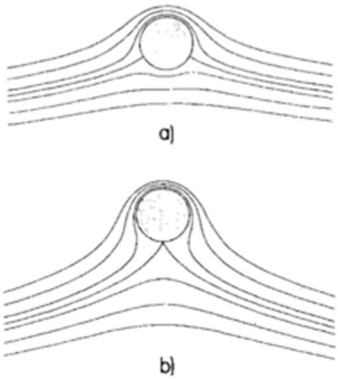

FIGURE 2. 2-D flow about a Cylinder

All these developments had one common goal, to raise the maximum lift coefficient higher and higher. A.M.O Smith [2] posed the question, "what is the maximum lift coefficient that can be generated?" He continued by explaining how inviscid two-dimensional flow around a circle, for which the circulation starts off weak (see FIGURE 2a) but continues to get stronger until it reaches maximum circulation which will cause both stagnation points to meet at the bottom of the cylinder (see FIGURE 2b). This would then result in the maximum section lift coefficient of a single element, found to be 4π using Joukowski airfoil theory [2]. This *CLmax* of ~12.6 is significantly larger than that typically attained. This is due to the inviscid assumption made; thus, the flow would not experience separation due to adverse pressure gradients. This of course is not a realistic assumption to make, but when trying to find the ceiling value of the lift coefficient (*CLmax*), these idealized assumptions can be made. This section lift coefficient ceiling quantifies how much high-lift devices can still improve, and as shown in FIGURE 3, a slow increase has been occurring over the years.

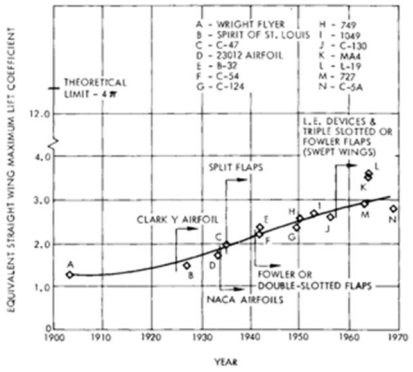

FIGURE 3. *CLmax* design trends [2]

B. Flow Separation

To fully understand flow separation over a body, it is important understand the nature of its boundary layer flow. As air travels over a body, frictional forces decelerate air in close proximity to the surface. Depending on the Reynolds Number, the boundary layer may comprise laminar (stratified) or turbulent (chaotically unsteady) local flow.

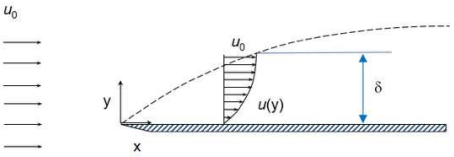

FIGURE 4. Boundary Layer [6]

In 1904 Prandtl presented a paper introducing his idea of the boundary layer [5]. He explained that at the surface of the body, the velocity of the flow must be zero, the no slip condition. As the flow travels further along the body, the loss of momentum near the surface of the body continues to grow causing the thickness of the boundary layer to increase; see FIGURE 4. [5]

From this, due to the relative thinness of the boundary layer, there must be a large velocity gradient for the flow inside of the boundary layer to achieve the velocity of the flow outside of the boundary layer**.** Due to the proportionality between shear stress and the velocity gradient, Prandtl concluded that the skin friction drag force exerted on a body was not negligible. [5]

Prandtl also described the event in which flow entering a zone of high pressure would "turn aside from it" due to a large momentum loss. [5] Here Prandtl was describing how an adverse pressure gradient causes flow separation. To provide more detail, lets observe the three basic cases for the flow across a body. The flow over a body can accelerate, decelerate, or have no acceleration, i.e., a constant velocity. The simplest

case is the constant velocity case. In this case, there is no pressure gradient, since the flow must experience zero acceleration, and thus the flow remains undisturbed and attached FIGURE 5b. The other case is when the flow is accelerating due to a favorable pressure gradient. In this case, as the name may hint at, the pressure gradient is helping the flow stay attached. Due to this, no separation will occur, and the boundary layer will be well rounded FIGURE 5a. The decelerating case proves to be the most interesting and complex of the three. In this case, there is an adverse pressure gradient on the flow slowing it down. As the adverse pressure gradient increases, the velocity gradient in the region close to the surface gets smaller and smaller. When the pressure gradient is sufficiently large, the flow separates as show in FIGURE 5c, d, e.

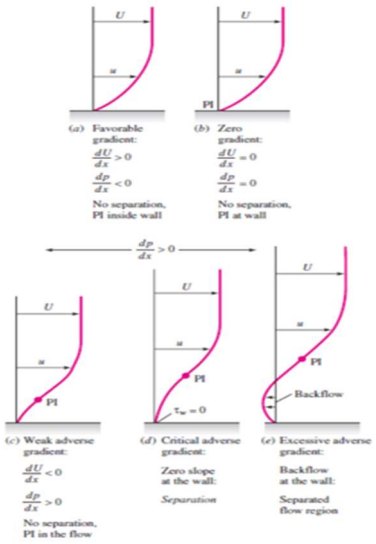

FIGURE 5. Boundary Layer Pressure Gradient Effects

Küchemann describes this in a quite intuitive manner [7]. He states that the slower particles in the boundary layer must overcome the same pressure rise as the faster particles in the outer stream. Both particles will be retarded due to the pressure gradient, but those in the boundary more so due to their lower kinetic energy. [7] Furthermore, Küchemann also explains how a thick boundary layer can more easily experience flow separation due to its larger region of low momentum flow near the surface of the body compared to thinner boundary layers. [7] Once separated, the boundary layer flow will deform and can even flow in the opposite direction as seen in FIGURE 5e, in this case there could even be a negative skin friction component for the separated flow. Although it may seem favorable to have negative skin friction, the benefits of this effect are rapidly outweighed by the loss of lift and higher pressure drag that also occur due to separated flow.

C. Flow Separation Over 2-D Airfoils

The separation of flow on airfoils stems from how lift is generated. In order to properly understand this, it is fundamental to understand how the characteristics of an airfoil affect the generation of lift. As the incoming free stream velocity reaches the body, the rounded leading edge of the airfoil turns the incoming flow causing a velocity increase. This increase in velocity is known as super-velocity [7] or perturbation velocity, and is a result of the thickness, camber, and incidence of an airfoil. As any of these three quantities on an airfoil increase, the super-velocities on the airfoil will also increase. At some point along the chord the local velocity, the sum of the free stream velocity and the super-velocity, will reach a maximum. Once the upper surface flow has traversed the whole airfoil, it will reconvene with the flow from the bottom surface at the trailing edge of the airfoil at a speed lower than that of the free stream [2]. Thus, the flow over an airfoil is first accelerated from free stream to a maximum velocity, and then decelerated to a velocity lower than free stream.

It is here where the problem arises. In order to increase lift, the pressure difference between the upper and lower surface of an airfoil must increase. For this to happen, greater velocities are needed on the upper surface of the airfoil. The greater the peak velocity is on the airfoil, the greater the declaration will be towards the trailing edge of the airfoil. As stated above, if the flow decelerates too quickly, it will separate.

III Development of an Integrated Potential Flow Tool which can Predict Flow Separation

A. Stratford's Method to Predict Flow Separation

Early flow separation prediction methods solved the momentum or energy equations in conjunction with expressions of the behavior and shape of the velocity profile [8]. While these methods proved to be accurate, they provided limited insight on the flow itself. In 1958, Stratford published a paper [8], which describes a method to predict the separation of the turbulent boundary layer.

$$\bar{C}_p \left(\frac{x d\bar{C}_p}{dx}\right)^{\frac{1}{2}} = 0.39(10^{-6}Re)^{\frac{1}{10}} \quad (1)$$

EQUATION 1 is Stratford's Method to predict separation of flows with Reynolds numbers of the order of 10^6. In this equation, x is the distance from the leading edge, $\bar{C}_p$ is the canonical pressure coefficient, and Re is the Reynolds Number of the flow. The limiting Stratford Separation Criterion in this form of the equation is 0.39.

$$S = \frac{\bar{C}_p\left(x\frac{d\bar{C}_p}{dx}\right)^{\frac{1}{2}}}{(10^{-6}Re)^{\frac{1}{10}}} \tag{2}$$

EQUATION 2 is obtained by rearranging EQUATION 1 algebraically. The limiting Stratford Separation Criterion of 0.39 is then replaced with the variable S, Stratford's Separation Criterion. At the leading edge, Stratford's Separation Criterion is equal to zero; it progressively increases as the flow traverses down the airfoil. Stratford's separation constant is thus the variable that is monitored along the flow, if it reaches the limiting Stratford separation value of 0.39, separation is said to occur.

There are other more involved methods to predict flow separation, such as Cebeci & Smith [9] or Presz & Pitkins [10], we selected Stratford's Method due to its simplicity and adequate accuracy.

B. Canonical Pressure Distributions

The typical pressure distribution is widely used, especially in any type of aerodynamic design work. Although pressure distributions provide great insight on the flow characteristics, the reader cannot, by inspection or simple calculation, determine much of the margin of safety of the boundary layer against separation. Due to this, a specific scaling is performed on the pressure distributions in the x and Cp directions. If the scaling is done properly, the result will be a "normalized" pressure distribution, referred to as a canonical pressure distribution which can then be used with EQUATION 2 to predict the location of flow separation. The advantage of the canonical pressure distribution, in terms of identifying the separation point, is that all the distributions are in a standard form FIGURE 6.

In this standard form, all canonical pressure distributions have $\bar{C}_p$=1 correspond to a stagnation point, the point where the local velocity is equal to zero, just like that on a typical pressure distribution. Furthermore, $\bar{C}_p$ =0 corresponds to the point at which the local velocity is maximum. [2][8] Relating this back to a typical pressure distribution, $\bar{C}_p$ =0 corresponds to the point C_{pmin}. This can be observed by comparing FIGURE 6a to FIGURE 6b. As shown in the canonical pressure distribution, the canonical pressure coefficient ranges from zero to one. In contrast, the typical pressure distributions ranges from one to about -0.8. If the angle of attack were to be increased, the canonical pressure distribution would still have the same canonical pressure coefficient range while the typical pressure coefficient range would increase.

In the standard form, the canonical pressure distributions are scaled by the peak velocity. As explained above, the deceleration of flow from this peak velocity down to a velocity lower than the free stream velocity at the trailing edge is what causes flow separation. Thus, scaling by this peak velocity results in the most favorable towards the analysis of flow separation. The scaling process begins with EQUATION 3, which shows the typical equation for the pressure coefficient:

$$C_P = \frac{P - P_\infty}{\frac{1}{2}\rho u_\infty^2} \tag{3}$$

Following Bernoulli's principle, EQUATION 4, the pressure coefficient can be re-written as EQUATION 5. It is important to note that the use of Bernoulli's equation implies the assumption of isentropic flow.

$$P_1 + \frac{1}{2}\rho u_1^2 + \rho g h_1 = P_2 + \frac{1}{2}\rho u_2^2 + \rho g h_2 \tag{4}$$

$$C_P = \frac{\frac{1}{2}\rho(u_\infty^2 - u^2)}{\frac{1}{2}\rho u_\infty^2} \tag{5}$$

It is here where the scaling can be easily shown. Instead of selecting the free stream velocity as the reference point, the maximum velocity point is selected. Thus, the free stream velocity, u_∞, is replaced with the maximum local velocity, u_0.

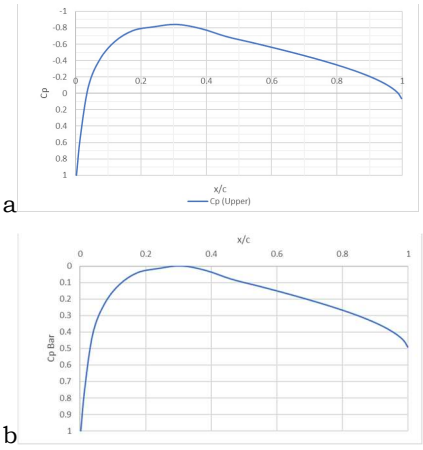

FIGURE 6. Pressure Distributions over a NACA 4412 2D airfoil at α=0°. a) Customary Cp, b) Canonical $\bar{C}_p$

$$\bar{C}_p = \frac{\frac{1}{2}\rho(u_0^2 - u^2)}{\frac{1}{2}\rho u_0^2} \tag{6}$$

$$\bar{C}_p = \frac{P - P_0}{\frac{1}{2}\rho u_0^2} \tag{7}$$

The result, EQUATION 6, is the equation for the canonical pressure coefficient. Using the same process as above it can be converted back to the conventional form, EQUATION 7. Here, we see that the only difference is the selection of the reference point.

In order to be able to quickly analyze the separation location, it would be beneficial to be able to convert from C_P to $\bar{C}_p$. This is mainly due to the ease of finding accurate pressure distributions using legacy potential flow codes. The conversion from typical to canonical pressure coefficients is mathematically simple, thus only a quick overview will be described. Starting with EQUATION 3, it is rearranged to equate to pressure, P. Substituting this into EQUATION 7 and following the same process as before using Bernoulli, as shown between EQUATION 3 and EQUATION 5, EQUATION 8 is obtained.

$$\bar{C}_p = \frac{\frac{1}{2}\rho u_\infty^2 C_p + \frac{1}{2}\rho u_0^2 - \frac{1}{2}\rho u_\infty^2}{\frac{1}{2}\rho u_0^2} \tag{8}$$

Here another assumption is added to the list, it is assumed that the flow is incompressible. This assumption simplifies EQUATION 8 to EQUATION 9 while also simplifying EQUATION 5 to EQUATION 10.

$$\bar{C}_p = \frac{u_\infty^2}{u_0^2}(C_p - 1) + 1 \tag{9}$$

$$C_P = 1 - \frac{u^2}{u_\infty^2} \tag{10}$$

Analyzing EQUATION 10 at the point of maximum velocity, u_0, results in the minimum pressure coefficient, $C_{P_{min}}$. The equation is then rearranged to equate the velocity ratio, this is then substituted into EQUATION 9 and simplified, the result is shown below in EQUATION 11.

$$\bar{C}_p = \frac{C_p - C_{p_{min}}}{1 - C_{p_{min}}} \tag{11}$$

EQUATION 11 is the final form used to convert C_p to $\bar{C}_p$. Here, the boundary limits of the canonical pressure distribution can be checked to ensure that EQUATION 11 is correct. At stagnation, $C_p = 1$, which would cause $\bar{C}_p = 1$. At the point of maximum velocity, $C_p = C_{p_{min}}$, thus the numerator of EQUATION 11 would go to 0, causing $\bar{C}_p = 0$. Both limits being the correct values mentioned earlier in this section. With a valid conversion between the two variables, there is now a need for accurate pressure distributions to be able to accurately predict the location of flow separation.

C. Potential Flow codes

During the 1970's, as computational technologies were advanced, the development of potential flow codes began. These "legacy" codes could solve the forces generated on an airframe relatively quicker compared to prior methods. During this same time, Luis Miranda wrote VORLAX, a vortex-lattice method code, for Lockheed under contract for NASA [11]. The use of VORLAX must be within acceptable Reynolds Number limits, typically $Re > 10^6$. VORLAX is a panel-based code, where the user inputs the physical geometry of an aircraft as a series of individual flat panels. VORLAX also has the capabilities for cambered and twisted flat panels. By combining sufficient flat panels, the geometry of an aircraft can be created FIGURE 7a, which yields excellent estimates of inviscid quantities, such as lift and stability moments. [2]

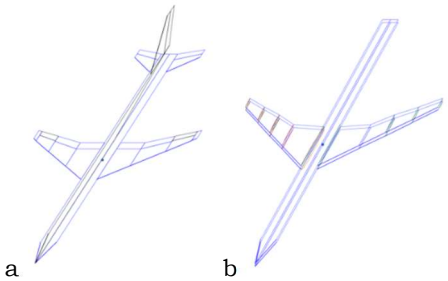

FIGURE 7: VORLAX models of a transport category aircraft wing/body. a) flat panel, b) sandwich panel

The advantage of using this code is the simplicity of it and ease to change the geometry being analyzed. Furthermore, VORLAX also has the capabilities to analyze more complex geometries. By using the "sandwich panel" feature in VORLAX, a thick wing can be properly simulated. The "sandwich panel" feature uses two single impermeable panels to simulate the upper and lower surfaces of a wing FIGURE 7b. As is typical in vortex-lattice codes, the single impermeable panels do not allow the flow inside

of the "sandwich" panel to affect the flow outside of the panels in any way. From this, accurate pressure coefficient distributions are outputted by VORLAX for the upper and lower surface of the "sandwich" panel at subsonic Mach numbers. [12][13] With these features, the user can analyze any wing with the desired thickness, camber, and local incidence (twist) along the span.

D. Assumptions made

This flow separation tool will be the main driver in determining the location at which the flow separates, thus the assumptions made while developing it must lie within reason for the specific situations which will be investigated. The following assumptions were made to develop the flow separation tool:

- The flow is isentropic
- The flow will have a Reynolds number in the order of 10^6
- The flow will be subsonic
- Once the flow separates, it is not able to re-attach

The focus of this paper is to investigate high-lift systems suitable for application on commercial transport aircraft. Assumption three is reliably applicable since high-lift devices are typically used during takeoff and landing; thus, the flow will most definitely be subsonic. Furthermore, due to the size of the aircraft being looked at, the Reynolds numbers will be sufficiently large to achieve accurate results. Isentropic flow is one where there are no irreversibility's and the flow is adiabatic. Due to the low speed being considered, irreversible and adiabatic flow are proper assumptions to make. During the discussion of VORLAX above, we noted that this code solves a purely inviscid phenomenon. This means that the drag it outputs is only induced drag, "drag-due-to-lift". This was not placed in the assumptions since the complete tool, the pairing of VORLAX with Stratford's Method, can account for flow separation. Thus, the output of the tool accounts for the viscous effect of concern in this paper. Lastly, the tool does not have the capability to account for flow re-attachment, thus it is assumed that once the flow separates, it will remain detached.

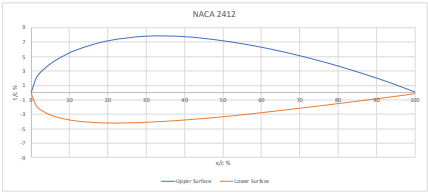

FIGURE 8. NACA 2412 Airfoil Profile

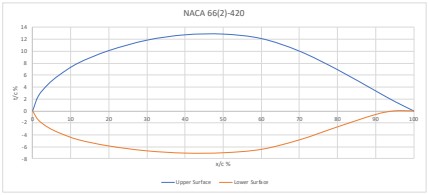

FIGURE 9. NACA 66(2)-420 Airfoil Profile

IV Stratford's Method Applied to 2D Airfoil Flow Problems

A. Single Element Airfoils

We first verify that the predicted location of separation made using Stratford agrees with published values. The first case that was run was to simulate an experimental study performed by Seetharam & Rodger for NASA Aeronautical Report 77-3 [14]. In this experiment, an oil/tuft study was performed to observe where the flow separation occurred on a NACA 2412 FIGURE 8. The Reynolds number of the experiment was 2.2 million, this was matched when simulated in the tool. The results from this experiment are shown in TABLE 1, included are also the results from the tool developed. As shown in the table, the experimental values in the NASA report were very similar. Although it is important to point out that the tool is slightly pessimistic, predicts flow separation early. Due to the limited quantity of points, more cases were run to verify the tool.

TABLE 1. NACA 2412 Experimental and Predicted Flow Separation Location

Angle of Attack	Experimental separation location (% chord)	Predicted separation location (% chord)
0	N/A	98
4	N/A	96
8	92.5	88
12	80	75
16	40	48

TABLE 2. NACA 66(2)-420 Experimental and Predicted Flow Separation Location

Angle of Attack	Experimental separation location (% chord)	Predicted separation location (% chord)
0	N/A	92
4	N/A	88
8	78	75
12	76	69
16	62	58
20	44	46
22	23	29

Our next simulation repeated the experiment performed by Cebeci & Smith under contract for the McDonnell Douglas Corporation [15]. In this experiment, a NACA 66(2)-420, FIGURE 9, was tested at a Reynolds number of 3 million. Once again, the Reynolds number was matched in the flow separation tool. The separation location results found in this experiment are shown in TABLE 2, included are the results from the tool developed. Like in the previous example, we see that the tool predicts flow separation slightly prematurely for low angles of

attack. Taking a closer look at TABLE 2, we see that as the angle of attack increases, and thus the onset of flow separation occurs earlier along the chord, the predicted values more closely match the experimental values. In the case of large angles of attack, $\alpha > 16^{\circ}$, the prediction of the flow separation by the tool is delayed. This is unacceptable, and thus the tool is limited to moderate angles of attack. Although, it is important to state that if only 50% of the chord has attached flow, the wing may be stalling or completely stalled. This is of great importance since at this range, the tool produces the most accurate results.

Thus, we see that the Stratford Method when applied to pressure profiles output from a potential flow code reasonably accurately predicts flow separation points. Thus, this combined method (proven out with 2D data) can now be applied to determine the "trust zone" of VORLAX. After sufficient flow separation, the wing will begin to experience stall, at which there is a significant loss of lift [7]. When this occurs, the lift coefficient values outputted by VORLAX can no longer be accepted as correct. Due to airfoils and wings having differing stall characteristics, a direct angle of attack cannot be specifically called out at which stall occurs. Instead, a more conservative approach will be taken. If the flow separates at a location of 50% to 70% of the chord, the corresponding range of angles of attack will be the limiting range of the VORLAX "trust zone". Thus, any solutions in this area could be invalid due to early stall onset.

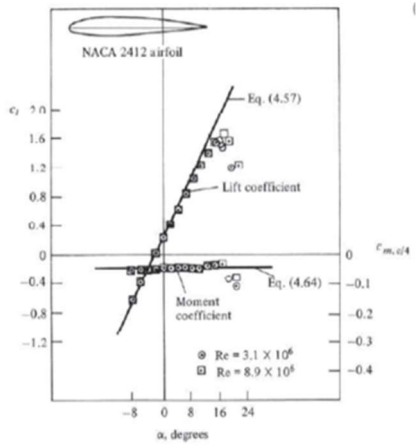

FIGURE 10: Sectional Lift Coefficient Curve for NACA 2412 [16]

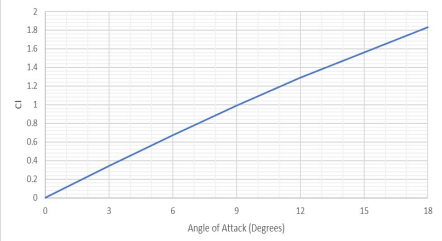

FIGURE 11: CL vs α for NACA 0012

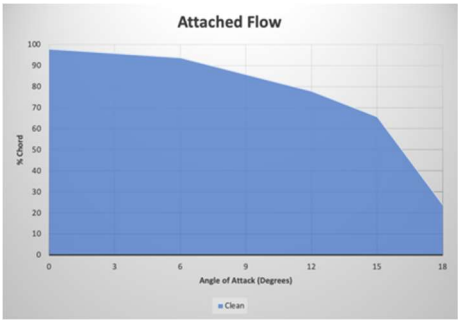

FIGURE 12: Attached flow over NACA 0012

To demonstrate the VORLAX "trust zone" observe the separation values in TABLE 1. The angle of attack at which 70% of the chord still has attached flow is slightly above 12˚. At the next angle of attack tested, flow separation is occurring at 48% of the chord. If this range, 12˚ to 16˚ angle of attack, is taken as the limiting range of the VORLAX "trust zone", then it is predicted that stall would occur somewhere in between these angles. Data for this airfoil was found in a classical textbook by Abbott and Von Doenhoff; see FIGURE 10 [16]. Observing the plot, we see that the lift coefficient begins to drop at 16˚, indicating the onset of stall. Once again, it is shown that the tool is conservative in predicting flow separation. Although it is beneficial to have a slight conservative prediction, to a limit, instead of having an optimistic prediction that does not capture flow separation when it occurs.

This next study begins with a simple airfoil, a NACA 0012 for its easily calculated camber and thickness profile, and obtain its section lift coefficient curve FIGURE 11.

While VORLAX outputs a well-defined linear lift prediction, due to the code's inviscid basis it cannot predict flow separation; thus it will produce inaccurate results at high angles of attack. At some angle of attack, there will be enough flow separation that the airfoil will begin to experience a loss of lift, stall. With the separation tool, we can identify the location at which the flow separates. At any location in front of this point, we assumed that the flow remains attached. Thus, to better show the separation point, a plot with the amount of attached flow will be created for a range of angles of attack FIGURE 12. In this plot, at an angle of attack of 12˚, the tool predicted flow separation to occur at 78% of the chord. Hence, on FIGURE 12, it can be observed that the flow remains attached up to 78% of the chord. On this plot, it is also shown that the flow significantly detaches at an angle of attack between 15˚ and 18˚. Thus, this is the limiting range of the trust zone for VORLAX. Observing FIGURE 11 once again, at a 15˚ angle of attack, the section lift coefficient is about 1.56. Observing test data in FIGURE 13, (overleaf) we see that experiments indicate that the loss of lift occurs at about 18 degrees angle of attack. Taken all together, it seems that Stratford's Method is accurate.

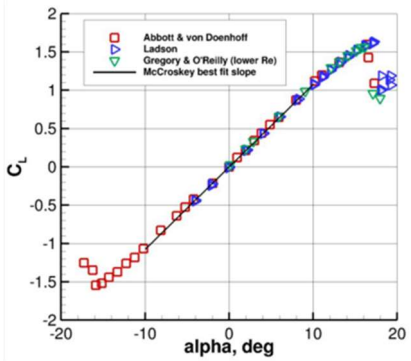

FIGURE 13: Sectional Lift Coefficient Curve for NACA 0012 [17]

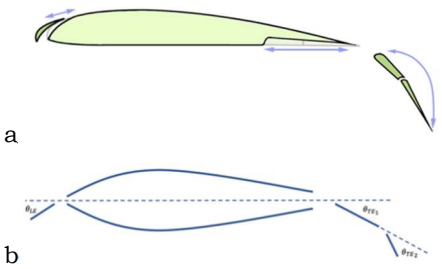

FIGURE 12: Airfoil with Double-Slotted Fowler Flap and Slat. a) physical geometry, b) VORLAX Quasi-Sandwich Panel Analog

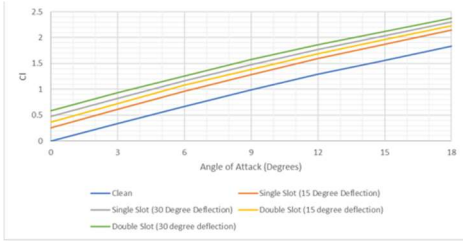

FIGURE 13: CL vs α for NACA 0012 with Trailing-Edge Devices

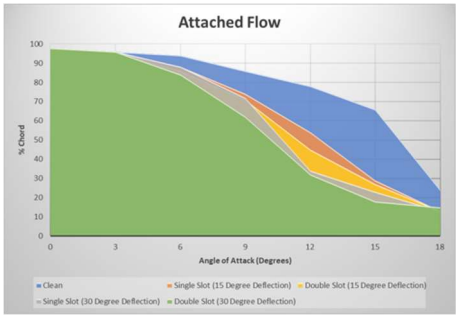

FIGURE 14: Attached Flow over NACA 0012 with Trailing-Edge Devices

B. Multi-Element Airfoils

When inputting the geometry of a high-lift system into VORLAX, multiple simplification must be made. Although the main wing can be simulated with VORLAX's "Sandwich" panel method, the leading and trailing-edge devices cannot. Instead, they are simulated with a single impermeable panel in front of or behind the main wing. Hence, a wing with double-slotted Fowler flaps and a slat FIGURE 14a would be inputted into VORLAX as seen on FIGURE 14b. Notice that the angle of deflection for either flap element can still be controlled in VORLAX as well as the slat angle deflection. Due to this simplification process, there is no difference in the geometry

From the multiple options of high-lift devices of interest, the investigation begins with trailing edge devices. To start off simple, a single-slotted Fowler flap is added to the trailing edge of the NACA 0012. The length of the flap is 25% of the chord, a typical value for this type of trailing edge device [18]. Furthermore, two different deflection angles will be tested. A moderate deflection angle, 15˚, and a high deflection angle, 30˚. Now the lift curve has the same slope but has been shifted upwards FIGURE 13. This is great, the airfoil is now producing significantly more lift at the same angles of attack.

Observing FIGURE 14, the addition of the trailing-edge flap has significantly affected the flow separation characteristics. The trust range limit for the lift outputted by VORLAX has now been decreased to an angle of attack between 9˚ to 12˚, compared to the 15˚ to 18˚ range for the clean airfoil. Looking back at FIGURE 13, this results in a sectional lift coefficient close to 1.3 for 15˚ flap deflection, and close to 1.5 for 30˚ flap deflection. Both values being similar to that of the clean airfoil, 1.5. Thus, although adding flaps shifts the sectional lift curve upwards, the earlier onset of flow separation the flaps induce limits the obtainable angle of attack and thus counteracts the increase in lift as shown in the example above.

For the case with double-slotted flaps, the flaps combined length was capped at the same 25% chord limit. Although, due to the possibility of overlap when stowed, double-slotted and triple-slotted flaps have the capability of further increasing lift, as a result of the further increase in chord when deployed. This is especially important for the triple slotted flaps, where the secondary flap elements tend to heavily overlap the main flap element when stowed. The effect of splitting the flap into multiple elements, which allows for greater deflections ultimately increasing the camber of the airfoil, can be observed in FIGURE 13. The effects of the additional camber are present and shown by the upwards shift in the lift coefficient curve.

The trends shown for the double-slotted flaps are very similar to those of the triple slotted flaps. Due to extreme overlap in FIGURE 14 when the triple flaps where included, those results were omitted. It was observed that if the total flap length remains the same size, the multi-element flaps induce flow separation slightly earlier on the main airfoil as their single element counterpart.

We showed that if the chord size remains the same, the flow separation behaves similarly for all three slotted flaps of interest. Although, what if the flap size were to be changed, how would the flow over the main airfoil change? A couple more cases were run to understand this, the single-slotted and double-slotted flaps at a 30˚ deflection were run but the size of the flaps was changed to be only 15% of the chord, referred to as "small flaps". The original 25% chord flaps run previously are referenced as the "large flaps". As we see in FIGURE 15, increasing the flap size from 15% to 25% chord length leads to earlier flow separation.

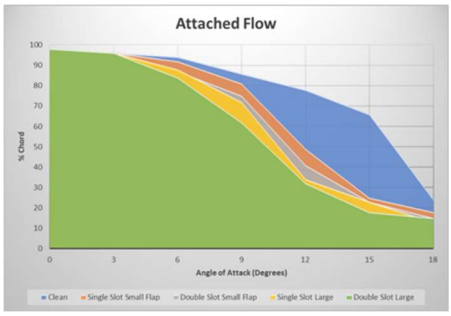

FIGURE 15: Attached Flow over NACA 0012 with Flaps at 30˚ Deflection.

As expected, due to the increase in flap length from the small to large flaps, the section lift coefficient increases as shown in FIGURE 16. The increase in lift coefficient was significantly larger when using the large flaps compared to the small flaps. This increase in lift coefficient was also drastically larger than that achieved by going from single to double slotted flaps with the same size chord and going from a flap deflection angle of 15˚ to 30˚. The drawback is that the space on an airfoil is limited, thus increasing the chord of the flap may not be an option.

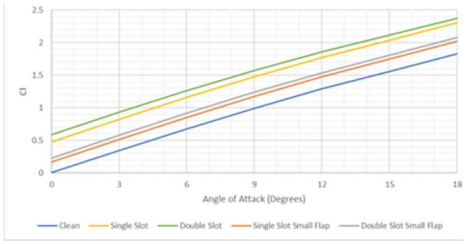

FIGURE 16: CL vs α for NACA 0012 with Flaps at 30˚ Deflection

The studies performed above show that the addition of only trailing-edge flaps to increase lift is neither efficient nor effective due to the early onset of flow separation at low angles of attack. This can be connected back to the super-velocities which develop over the upper surface of the wing. As the local velocity on the upper surface of the wing becomes larger, the pressure decreases and so does the pressure coefficient. Therefore, the lower the pressure coefficient, the faster the flow is traveling at the location of peak suction. Due to the flow having to decelerate, significantly large (large negative number) peak pressures very close to the leading edge of the wing are an indication of possible flow separation. This, of course, is not a proper way to evaluate the flow separation problem, it is merely a qualitative observation after performing numerous amounts of studies like the one above. Furthermore, let this not be confused with the highly beneficial "peaky" pressure distributions as explained by Pearcey [19]. For example, in the study performed above, the pressure distribution for the NACA 0012 airfoil, at a three-degree angle of attack, has a well-defined peak at about 10% of the chord with a peak suction pressure coefficient of about -0.85 FIGURE 17. When the angle of attack reaches 15 degrees, the peak suction pressure coefficient has been reduced to almost negative four and pushed forward to about two percent of the chord FIGURE 18.

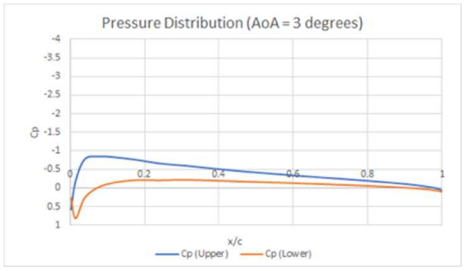

FIGURE 17: Cp Distribution for NACA 0012 at α =3˚

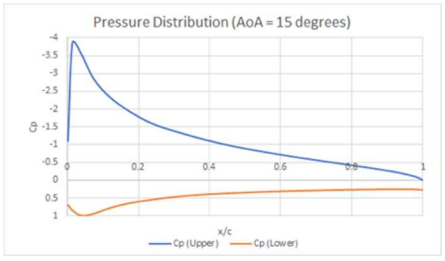

FIGURE 18: Pressure Distribution for NACA 0012 at α=15˚

To reduce separation associated with the leading edge suction peak, we next add a leading-edge device. To better show the effects of each leading-edge device, the 25% chord flaps will be used with 30˚ deflection angle. In the previous study this was shown to be the case that induced the earliest flow separation. Here we add a leading-edge element with a gap (a "slat") and one without a gap (a "Krueger Flap").

The results for the airfoil with slats show that the addition of this leading-edge device is tremendously helpful in keeping the flow attached. FIGURE 19 shows that when the slat is fully deflected (30˚ drooped down), the VORLAX trust zone increases up to 15˚ to 18˚. Moderate deflections of the slat, 15˚ deflection, performs well but is not able to provide as much pressure relief as the further deflected slat.

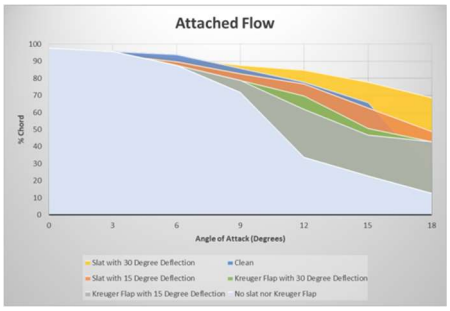

FIGURE 19: Attached Flow over NACA 0012 with Single Slotted Flaps at 30˚ Deflection and 30˚ Deflection Leading-Edge Device

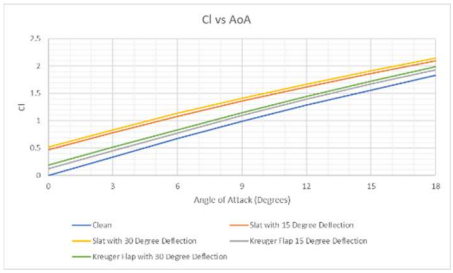

FIGURE 20: CL vs α for NACA 0012 with Single Slotted Flaps at 30˚ Deflection and Leading-Edge Devices

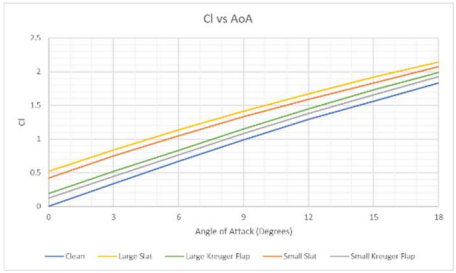

FIGURE 21: CL vs α for NACA 0012 with Single Slotted Flaps at 30˚ Deflection and Slats or Krueger Flaps

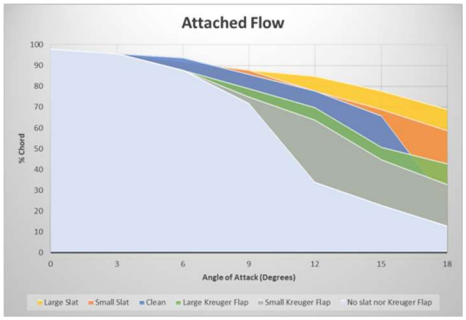

FIGURE 22: Attached flow for NACA 0012 with Single Slotted Flaps at 30˚ Deflection and Slats or Krueger Flaps

Observing the limit of the VORLAX trust zone on FIGURE 20, it is shown that the wing with the slats is producing significantly more lift now while still having sufficient attached flow. The airfoil with the slats at 30˚ deflection can reach an 18˚ angle of attack at which point it produces a section lift coefficient of about 2.1 while still having attached flow on 70% of the chord. At this same angle of attack, the airfoil with a slat deflection of 15˚ has attached flow on about 50% of its chord signifying that it is no longer in the VORLAX trust zone and may be experiencing stall. The airfoil with a smaller slat deflection is still an improvement over the clean airfoil since its flow separation characteristics are very similar to those of the clean airfoil, but with significantly higher sectional lift coefficient.

The same two studies were performed with the simulated Krueger flap eliminating the gap. As shown in FIGURE 20, the Krueger flaps significantly underperform when compared to the slats. The Krueger flaps shift the sectional lift curve slope upwards from the clean airfoil design but fail to even meet 50% of the delta Cl obtained by the slats. For example, the airfoil with slats produces a sectional lift coefficient of about 0.8 at 3˚ angle of attack. In order to obtain the same lift coefficient on the airfoil with Krueger flaps, an angle of attack of 6˚ would be needed.

The part of the study that is even more worrisome is the effect of Krueger flaps on the flow separation. Both runs for the Krueger flaps, 30˚ and 15˚ deflection, fail to provide enough relief to the main airfoil, refer back to FIGURE 19. Overall, even though the Krueger flaps are an upgrade from having no leading-edge device, they are heavily outperformed by the slats

The last effect to check is how the flow separation characteristics are changed by varying the size of the leading-edge devices. For this, the 15% chord slat and Krueger Flap were reduced to only 7.5% of the chord. In this study, the 30-degree deflection case for the leading-edge devices was run since it provides the most relief to the main wing. Again, increasing the size of the leading-edge device increases the sectional lift coefficient significantly more than increasing the deflection FIGURE 21. Although, the main advantage of increasing the slat deflection is that it provides greater pressure relief to the main airfoil. Comparing FIGURE 22 with FIGURE 19, we see that even though the slat is smaller in this study, since it is deflected 30˚, it provides more relief to the main airfoil than the larger slat deflected only 15˚ in the previous study.

C. Observations for High-Lift Systems in 2-D Flow

These studies gave us great insight into the basics of High-Lift Systems. We observe that in order to generate an increase in lift, both leading-edge and trailing edge devices should be employed. Whenever a trailing edge device is added to an airfoil, it severely affects the flow over the main element where the added area and camber leads to premature flow separation. Leading-edge devices can be used by themselves to prevent flow separation, but they don't provide sufficient increase in lift when compared to airfoils with flaps. Furthermore, the induced flow separation occurs quicker when going from single to double to triple slotted flaps. The

difference between these is relatively small and due to the increase in camber caused by the additional deflection as more elements are added to the fowler flaps. Even with this effect, the slat can relieve the pressure peak on all three flap systems and delay flow separation. The same cannot be said about the Krueger flaps. The Krueger flaps do not provide the sufficient relief to the main airfoil in terms of flow separation and severely lack performance in generating additional lift.

Up to this point, the term "relief" has been used to explain the effect the slat has on the main airfoil. Due to the importance of this effect, it is important to clarify that this term is used as an umbrella term to describe multiple effects. The main ones being the dumping effect, the slat effect, and the fresh boundary-layer effect. The dumping effect is a result of the slat having larger velocities in the boundary layer that are "dumped" onto the element aft of it. This dumped high velocity reliefs the pressure rise on the airfoil since it is the element aft of the slat. The slat effect is a result of the circulation velocities on the slat being in the opposite direction of the velocity on the main wing. This also aids in reducing the pressure peaks on the airfoil. Lastly, the fresh boundary layer is the property that every element of a wing with a slot in front of it starts off with a new boundary layer. Due to this, these boundary layers are thinner which means they are more resistant to adverse pressure gradients. In order to be more concise throughout this paper, the term "relief" has been used and will continue to be used to describe the three effects described above.

V Stratford's Method Applied to 3D Finite Wing Flow Fields

A. Need of 3-D Analysis

As we demonstrated in Section IV, the basics of high-lift systems can be simulated with ideal 2-D flow simulations. Although these simulations provide good insight into the characteristics of the flow, they don't account for the highly important three-dimensionality effects in aerodynamics. The process to analyze these systems in 3-D flow increases the complexity of the problem, but this study would be tremendously incomplete without it due to the demonstration by Jensen & Takahashi [20], in which a significant difference between analyzing a purely 2-D model and a 3-D wing section was shown. Due to this, the analysis of the 3-D flow must be studied to completely understand the aerodynamics of high-lift systems and the design decisions made on commercial transport aircraft.

All the studies presented in this section model a wing/body lifting system; see FIGURE 23, in order to capture the effect a fuselage has on the flow over the wing.

There is a total of five control points on all the wings that will be studied. At these control points any property of the wing can be changed such as local incidence, camber, thickness, sweep, etc. The first point is located at the side of body, the second point is located at the midpoint between the midspan and the side of body "inner midspan", the third point is located at the midspan, the fourth point is located at the midpoint between the midspan and the wing tip "outer midspan", and the fifth and final point is located at the wing tip.

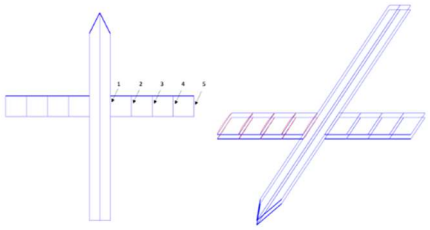

FIGURE 23: VORLAX Visualizer with Control Points Marked

B. Simple Wings with High-Lift Systems

The study begins once again with a simple case, a "Hershey Bar" wing with no local incidence (twist), an aspect ratio of 9, and the same NACA 4412 airfoils along the span. The simulation is run at an angle of attack of 3˚ at Mach 0.25 at an altitude of 4000 ft using the corresponding standard day table values for this altitude. [21] The outputs of the tool are now different, in order to capture the entire flow over the wing, pressure coefficient and flow separation contours are plotted. The pressure coefficient contour is made by obtaining all pressure coefficient values outputted by VORLAX. On the pressure coefficient contours FIGURE 24a, blue signifies low pressure zones while red signifies high pressure zones. The flow separation contour is made by applying the tool to every chordwise line along the span. On the flow separation contours FIGURE 24b, it is important to note than any shade of red signifies that the flow has separated. The color bar was locked so that red corresponds to a Stratford Separation Criterion of 0.39 or greater. Both plots begin at a span of about five feet since the simulation was run with a 10-foot-wide fuselage.

As seen in FIGURE 24b, the flow remains attached up to about 92% of the chord for most of the span for the "clean" wing case. In contrast, the pressure distribution is not constant along the span varying significantly, as a result of making the span finite. There is an area of peak pressure coefficients spanning the inboard and mid-section of the wing represented by the dark blue isobar FIGURE 24a. To further show

this in detail, FIGURE 25a-e presents the developed pressure distribution across each of the five control points. We observe hat close to the side of body, the peak under pressure coefficient is about -0.8. Moving along the span, the pressure coefficient peaks in the inner midspan section of the wing at a pressure coefficient of about -0.9. From that point on the peak pressure coefficient increases, until it reaches a value of about -0.5 at the wing tip.

The same "Hershey Bar" wing is now simulated with all the same conditions, the only difference being an increase in angle of attack to 9˚. With this increase in angle of attack, the peak under pressure coefficient has now increased to about -1.8 as can be seen on the color bar limit. Furthermore, the peak pressure coefficient area on the wing has moved towards the leading edge and root of the wing as shown by the dark blue isobar FIGURE 26A, overleaf. This has caused an early onset of flow separation near the wing-root as shown in FIGURE 26B. The trend observed here was also found in 2D flow: as the peak suction grows stronger and closer to the leading edge, it is more likely that the flow begins to experience separation.

The same wing is now raised to a 15˚ angle of attack. Observing the color bar limits, it can be observed that the peak under pressure coefficient is now reaching values close to -3.7, see FIGURE 27a. The peak pressure area has been pushed so far forward and towards the root that the dark blue isobar can barely be seen on the upper left corner. The peak pressure coefficient being so close to the leading edge and so large has caused the flow to separate at about 50% of the chord for most of the inboard section of the wing. The wing tip is still experiencing mostly attached flow, as has been the case in the previous two runs.

At this point the wing is experiencing sufficient flow separation to stall the inboard section of the wing. By adding a trailing edge flap and leading-edge slat, the wing will be capable of producing more lift while also delaying flow separation, as shown in the 2D case. Hence, both devices were added to the "Hershey Bar" wing to observe how it would affect the flow characteristics. The slat added was 15% of the chord and was deflected 30˚ while the flap

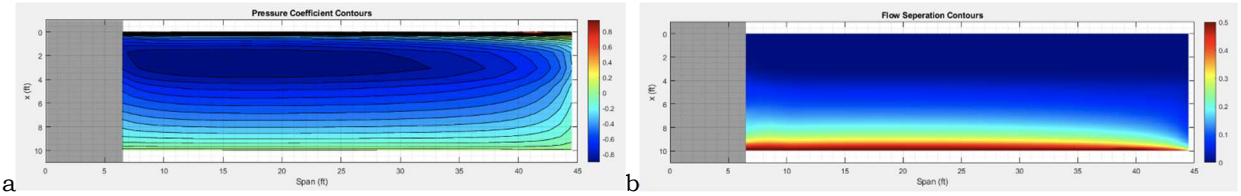

a b

FIGURE 24: NACA 4412 "Hershey Bar" Wing α=3˚. a) *Cp* contours, b) Stratford *S* Criteria

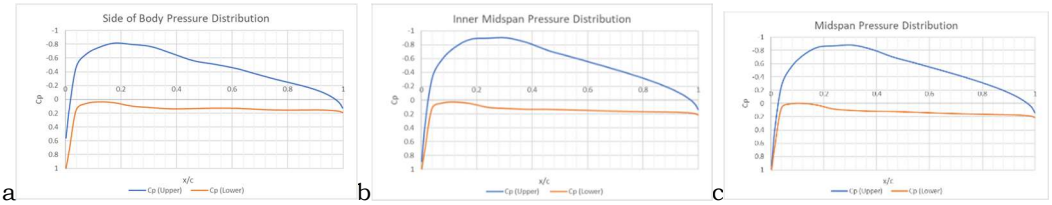

a b c d e

FIGURE 25: *Cp* Distribution for NACA 4412 "Hershey Bar" Wing α=3˚ at various spanwise locations. a) side-of-body (control point 1), b) inner-midspan, c) midspan, d) outer-midspan, e) wingtip.

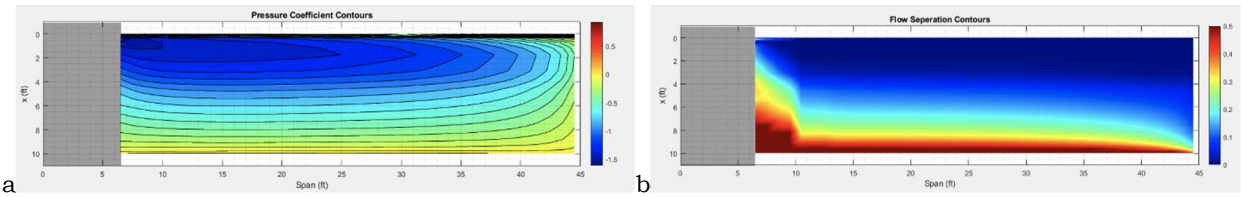

a b

FIGURE 26: NACA 4412 "Hershey Bar" Wing α =9˚ a) *Cp* contours, b) Stratford *S* Criteria

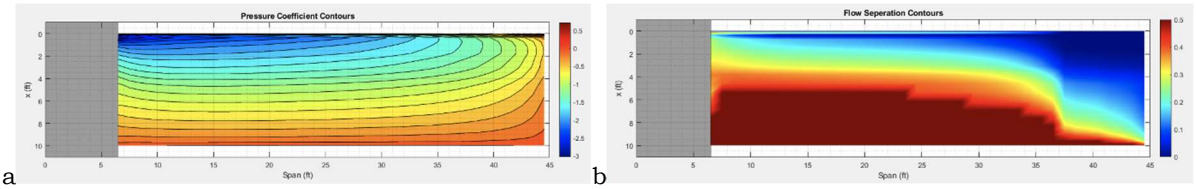

a b

FIGURE 27: NACA 4412 "Hershey Bar" Wing at α=15˚ a) *Cp* contours, b) Stratford *S* Criteria

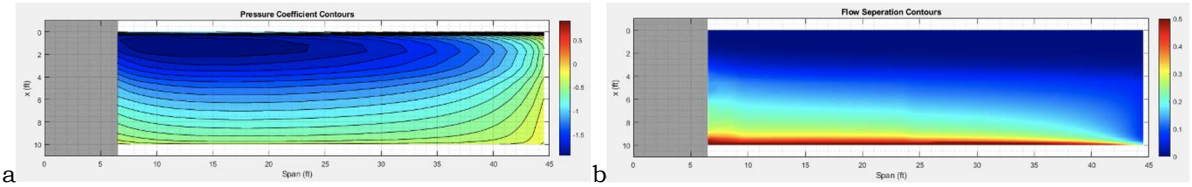

a b

FIGURE 28: NACA 4412 "Hershey Bar" Wing α=15˚ with Slats and Full-Span Single Slotted Flaps a) *Cp* contours, b) Stratford *S* Criteria

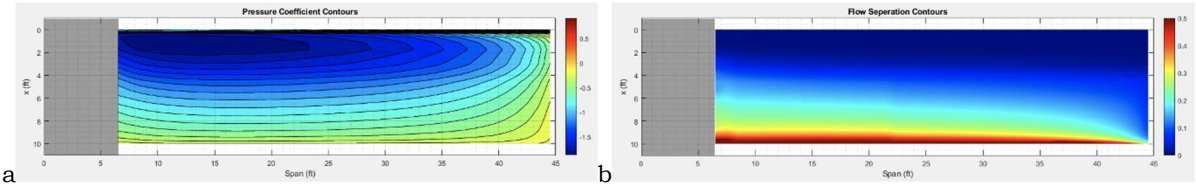

a b

FIGURE 29: NACA 4412 "Hershey Bar" Wing α=15˚ with Slats and Full-Span Double Slotted Flaps. a) *Cp*, b) Stratford *S* Criteria

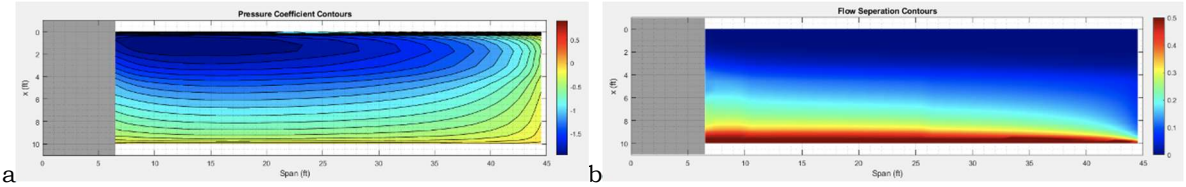

a b

FIGURE 30: NACA 4412 "Hershey Bar" Wing at α=15˚ with Slats and Full-Span Triple Slotted Flaps a) *Cp* contours, b) Stratford *S* Criteria

added was 25% of the chord and had a deflection of 30˚ as well. The pressure coefficient contour for this set up is shown in FIGURE 28a. Comparing this to FIGURE 27, we see that the slat is providing relief to the wing causing a shift of the minimum pressure coefficient area aft, towards the trailing edge of the wing and stretching the area towards the tips as shown by the dark blue isobar FIGURE 28a. Checking the limits of the color bar, it can also be observed that the peak pressure coefficient has been reduced to about -1.8. In order to check if the pressure relief was sufficient, the flow separation contour FIGURE 28b is observed. This shows that the flow is remaining attached for most of the chord along the span, with the flow separating at about 96% on the inboard and 98% on the outboard wing section.

The same slats were kept on the wing, but the trailing edge flap was changed to a double slotted flap. This flap was still the same size, 25% of the chord, with the main flap element being 70% of this length and the secondary flap element being 30% of this length. The result of this setup FIGURE 29A is very similar to that of the single slotted flap, the main difference being that this setup experience flow separation at about 94% of the chord in the inboard section and 96% of the chord on the outboard section of the wing FIGURE 29B.

Finally, we examine triple slotted flaps; this flap was also kept at a size of 25% of the chord with the main flap element being 60% of this length and the secondary elements being 20% of this length each. Once again, these results are very similar to those found in the previous two cases FIGURE 30a. With the main difference being where the location of flow separation occurs. For this case, separation occurs at 92% of the chord on the inboard and 95% on the outboard section of the wing FIGURE 30b.

All three of the cases above experience very similar flow separation characteristics as well as pressure distributions; their differentiating factor is their performance in generating Lift. As we see in TABLE 3, as more elements are added to the flap, the wing is able to produce more lift. This being due to the increase of camber on the wing due to the larger flap deflections possible when the flap has more elements. Although, it is this same effect that adds significant induced drag to the wing. The force over an element acts normal to its surface, thus when an element is heavily deflected, only part of the force being generated is in the upwards direction. For example, in FIGURE 31, as the elements are deflected further and further, the normal direction begins to point less and less upwards. Thus, if that element is generating some force, only a portion will be going towards lift, the rest will be going into drag. Therefore, even though flaps with more elements and/or deflection are capable of producing more lift, they will also experience severely higher drag.

TABLE 3. Lift for a NACA 4412 "Hershey Bar" wing at α =15˚

Wing	CL
Clean Wing	1.53
Wing with Single Slotted Flap	2.66
Wing with Double Slotted Flap	2.95
Wing with Triple Slotted Flap	3.05

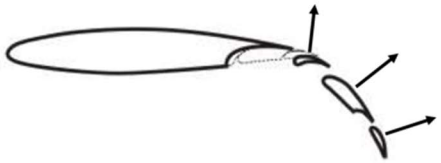

FIGURE 31: Normal Force Direction on the Flap Elements of Triple Slotted Flaps

C. Effects of Wing Sweep on Flow Separation

In order to achieve competitive speeds, transport aircraft utilize wing sweep. Furthermore, due to the landing gear implementation and structural wing advantages, most transport aircraft also have a Yehudi, an extension of the chord near the side of body of the aircraft FIGURE 32. In order to see the effects that wing sweep has on flow separation, multiple cases were run with varying sweep angles. In order to easily compare the effects, the most demanding case in the previous study was utilized, the triple slotted flap. Furthermore, to more clearly see the flow separation effects, a smaller less deflected, 10% the chord with a deflection of 20˚, slat will be used.

FIGURE 32: Yehudi on a Boeing 777-200

We re-ran the "Hershey Bar" with the smaller slats to establish a basis for the swept wings. To re-iterate, the size of the slat was reduced from 15% of the chord to 10% of the chord and the deflection angle was reduced from 30˚ to 20˚. By decreasing the size and deflection of the slat, it no longer provides enough relief to the wing. The peak pressure coefficient on the pressure contour has shot up to about -2.5 as seen on the color bar limit FIGURE 33a. Furthermore, the wing is experiencing significantly less attached flow, with separation occurring at 70% of the chord on the inboard section and moving back to 80% at the mid-span of the wing FIGURE 33b.

We next modify the geometry to incorporate 25˚ leading-edge sweepback; all other parameters are kept the same. With the increase in sweep, the minimum pressure coefficient decreases slightly from -2.2 to about -2.1 while the minimum pressure area, the dark blue isobar, shifts even further outboard FIGURE 34a. The flow separation characteristics have also changed, flow separation is now being observed in the mid-span area, still at the 70% chord location FIGURE 34b. Another flow separation characteristic occurs in the Yehudi, in which the flow is now experiencing very little detached flow. This being due to the extension of the chord in the Yehudi; the larger chord provides the flow more distance to decelerate, thus separation is less likely to occur.

This next case sweeps the same wing at an even more aggressive sweep angle of 40˚. The same trends can still be observed in this case, like the minimum pressure coefficient being slightly larger at about -1.8 compared and the minimum pressure area being stretched along the span towards the outboard of the wing FIGURE 35a. Furthermore, this case also shows how an increase in sweep, increases the spanwise size of the section experiencing the earliest onset of flow separation, still at 70% of the chord. Observing FIGURE 35b, this section spans about 20 ft, from 17 to 37 ft while in the case with 25˚ it spans about 15 feet, from 17 to 32 ft FIGURE 34b.

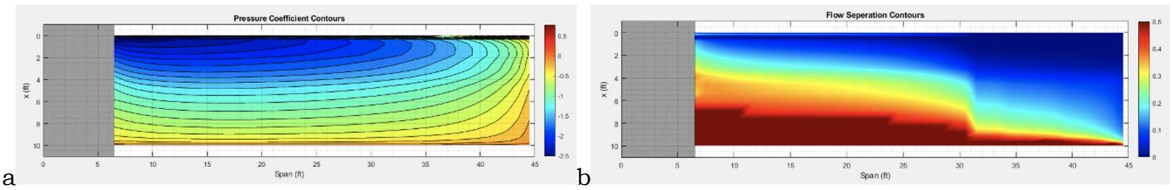

a b

FIGURE 33: NACA 4412 "Hershey Bar" Wing α=15˚ with 10% Chord Slats and Full-Span Triple Slotted Flaps. a) *Cp* contours, b) Stratford *S* Criteria

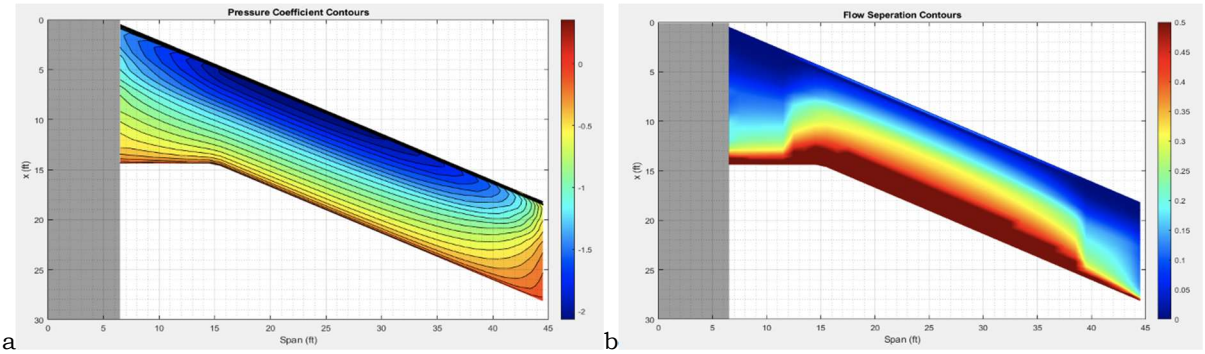

a b

FIGURE 34: NACA 4412 25˚ Swept Wing α =15˚ with 10% Chord Slats and Full-Span Triple Slotted Flaps. a) *Cp* contours, b) Stratford *S* Criteria

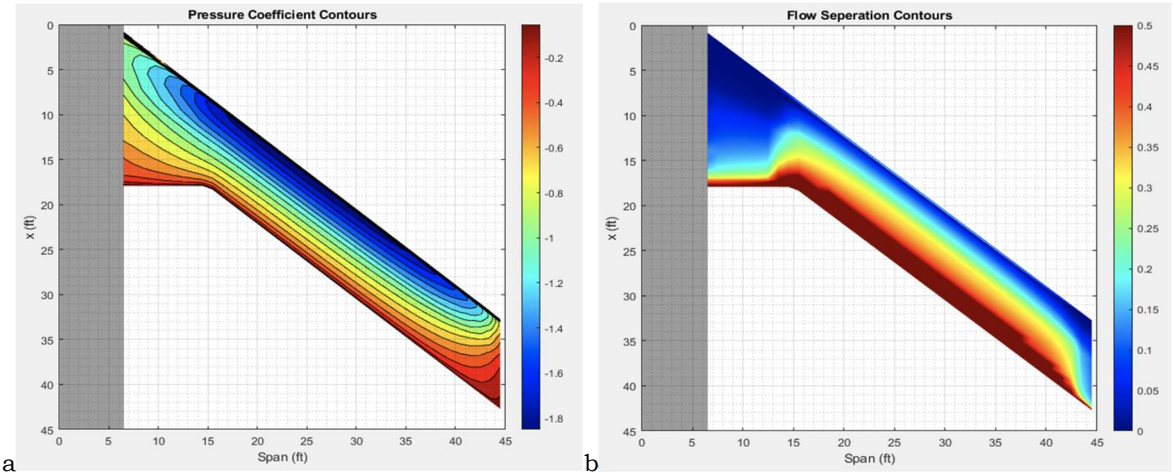

a b

FIGURE 35: NACA 4412 40˚ Swept Wing α=15˚ with 10% Chord Slats and Full-Span Triple Slotted Flaps a) *Cp* contours, b) Stratford *S* Criteria

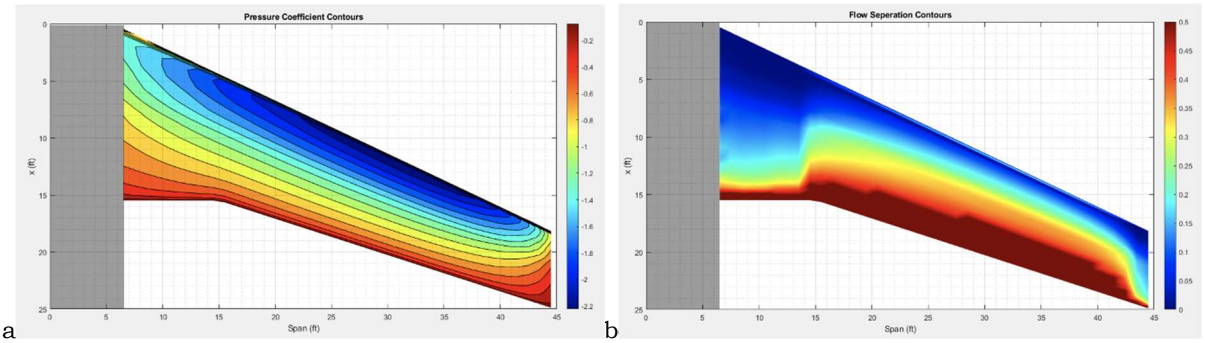

a b

FIGURE 36: NACA 4412 25˚ Swept and TR=0.5 Wing α =15˚ with 10% Chord Slats and Full-Span Triple Slotted Flaps a) *Cp* contours, b) Stratford *S* Criteria

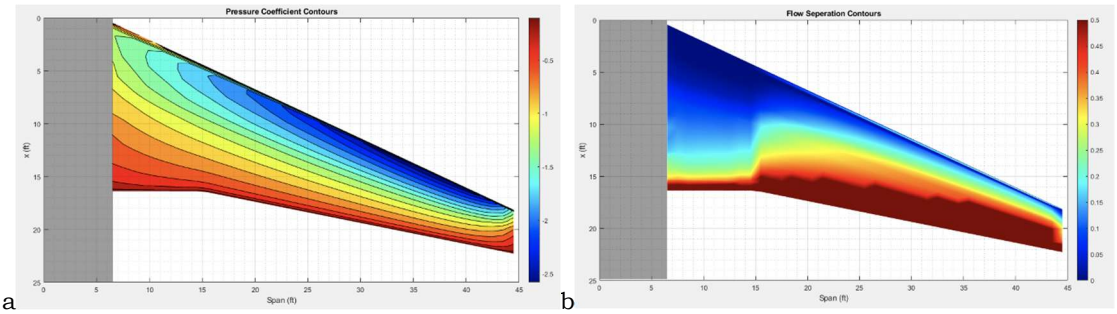

a b

FIGURE 37: NACA 4412 25˚ Swept Wing TR=0.25 α=15˚ with 10% Chord Slats and Full-Span Triple Slotted Flaps a) *Cp* contours, b) Stratford *S* Criteria

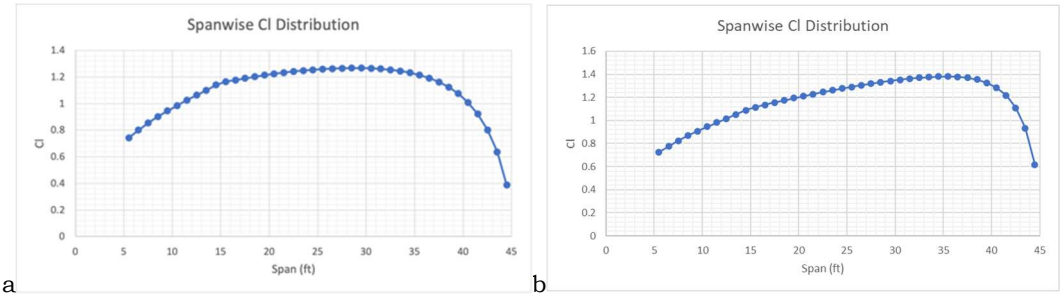

a b

FIGURE 38: Sectional Lift Distribution of Untwisted Wing at α=15º. a) TR=0.5, b) TR=0.25

D. Effects of Taper Ratio on Flow Separation

The taper ratio of a wing is the ratio between the tip and root chord. Wings are tapered to increase their efficiency as well as for structural purposes. The effects of taper ratio on flow separation will be studied using the same wing that was used in the previous study, specifically the one with 25˚ of wing sweep FIGURE 34a and FIGURE 34b. The first case that will be looked at is keeping all parameters the same but decrease the taper ratio to 0.5. In order to keep the reference area, the same, the root chord was increased to about 13.33 ft while keeping the taper ratio at 0.5, all other parameters where kept the same. This case produces results with some important differences when compared to the previous case. In this case, the minimum pressure area is moved outwards towards the wing tip FIGURE 36a, prior page. This results in the onset of flow separation area, occurring at 70% of the chord still, to move further towards the tip FIGURE 36b. This effect should be avoided due to the instabilities that result from wing tip stall and the loss of roll control.

In order to view the effect of even more aggressive taper ratios, the case below was run with a taper ratio of 0.25. Again, in order to keep the reference area constant, the root chord was further increased to 16 ft. With this set-up, the effects of reducing the taper ratio are more apparent. With this taper ratio, the minimum pressure coefficient has decreased to about -2.5 and the minimum pressure area has been pushed very close to the wing tip shown once again by the dark blue isobar FIGURE 37a. Furthermore, the wing is now experiencing the eeliest onset of flow separation on the wing tip, at about 44% of the chord FIGURE 37b. This effect is once again due to the chord of the wing. As the taper ratio decreases, the physical size of the chord on the outboard section of the wing is smaller. Hence, the chord must decelerate much quicker triggering the flow to separate.

The effect shown above can be connected to the effect tapper ratio has on the sectional lift coefficient distribution. As taper ratio decreases, the peak sectional lift coefficient moves outboards on the span. For the wing with a taper ratio of 0.5, the sectional lift coefficient peaks at about 60% of the span with a value of 1.25 FIGURE 38a. The wing with a smaller taper ratio, 0.25, has a peak sectional lift coefficient of about 1.4 which occurs at about 80% of the span FIGURE 38b. These high sectional lift coefficients on the outboard section of the wing will likely cause stall, just like predicted by the tool above.

E. Effect of Twist on Flow Separation

It is common to introduce local incidences, twist, on a wing design to obtain the optimal performance. The more common type of twist on transport aircraft is wash out. This being the application of positive incidence,

leading edge up, at the inboard section of the wing. The incidence is then progressively decreased until a negative incidence, leading edge down, is obtained at the wing tip [18]. This type of twist is quite beneficial towards flow separation since the tip of the wing is experiencing a lower angle of attack which delays the onset of flow separation in this vital wing area. To show this effect, the case above for FIGURE 37 is rerun implementing a simple washout twist: +6˚ at the side of body, +2˚ at the inner midspan, 0˚ at the midspan, -2˚ at the outer midspan, and -6˚ at the wing tip. This change in twist has increased the minimum pressure coefficient from -2.5 to -2.2. The minimum pressure area has also been pushed back towards the midspan section of the wing FIGURE 39a. In terms of flow separation, the large amount of detached flow at the wing tips has disappeared and the flow now remains attached up to the 70% chord mark FIGURE 39b. We see the benefits of the wash out twist when we compare FIGURE 37a and FIGURE 37b.

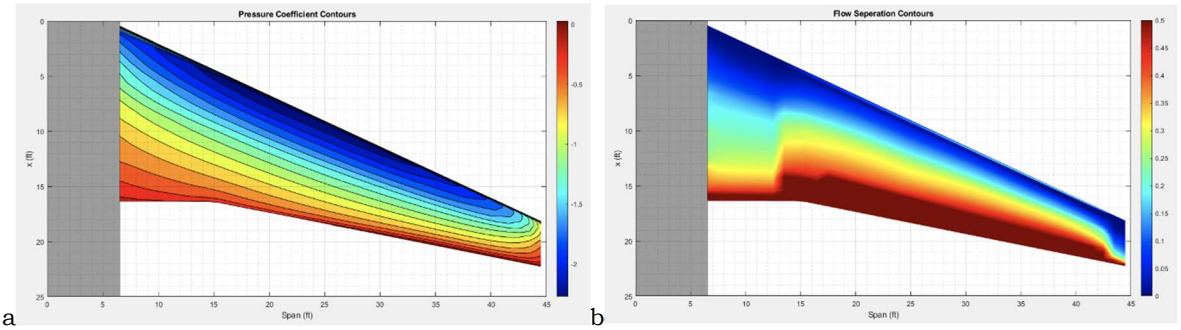

a b

FIGURE 39 NACA 4412 25˚ Swept Wash-out Twisted Wing TR=0.25 α =15˚ with 10% Chord Slats and Triple Slotted Flaps. a) *Cp* contours, b) Stratford *S* Criteria

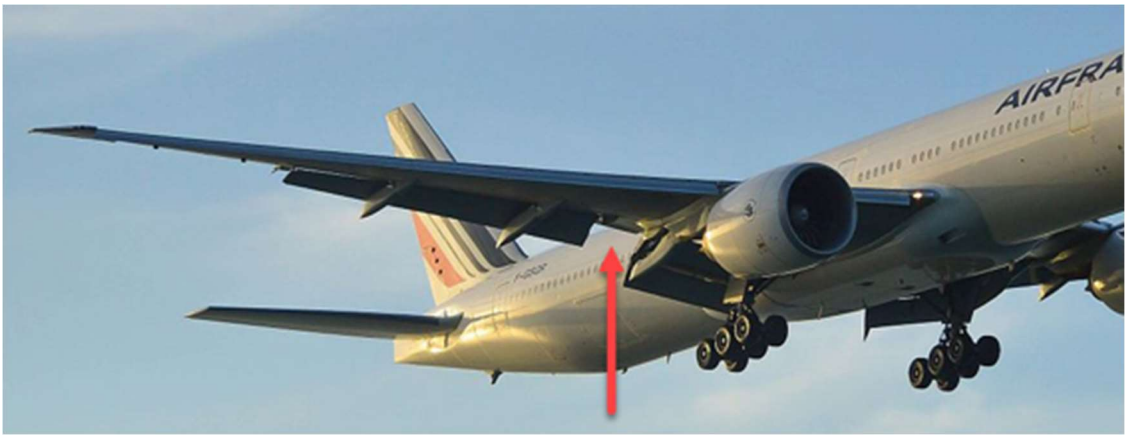

FIGURE 40: Thrust Gate on a Boeing 777

F. Effects of Interrupted Flaps

We must also consider other aspects of the wing that need to be included, like the fact that these types of aircraft do not have a flap along the entire span. Multiple Boeing transport aircraft boast a thrust gate like the 777 FIGURE 40 to keep hot exhaust gasses away from deflected flap structure.

We investigate interrupted-flaps by re-running the case above with wash-out twist but with no flap paneled in the wing section right after the Yehudi. The effect of this can be observed in FIGURE 41a, where the isobars at this location have been deformed by being pushed forward. This deformation leads to changes in the flow separation characteristics. FIGURE 41b shows how the area with the missing flap has flow separation occurring earlier along the chord. Thus, flap interruptions tend to negatively affect the flow separation characteristics. It is for this reason, although not solely due to this, that other aircraft manufactures, like Airbus, prefer the uninterrupted flap design. It also explains the reason why Boeing started using flaperons on aircraft with high-speed ailerons.

A flap interruption that is present on most commercial transport aircraft is that of the outboard ailerons. The wing tip trailing edge area is occupied by the ailerons and thus a flap cannot be present there. To simulate this, the outermost flap panel is removed from the simulation. This has the same effect on the isobars of the wing as the midspan flap interruption FIGURE 42a, although less noticeable due to the tip

effect. This results in the wing tip experiencing flow separation onset before any other section of the wing once again FIGURE 42b. Unfortunately, unlike the previous aspects which could be changed to prevent flow separation on the wing tip, ailerons are a vital control surface needed for the airframe to be stable and controllable. Thus, this effect is typically mitigated with a larger slat at the outboard section of the wing.

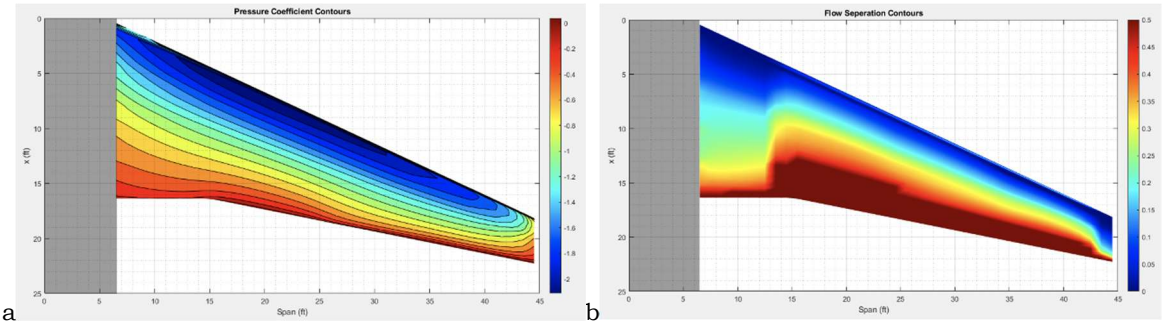

a b

FIGURE 41: NACA 4412 25˚ Swept Twisted Wing with TR=0.25 α =15˚ with 10% Chord Slats and Interrupted Triple Slotted Flaps. a) *Cp* contours, b) Stratford *S* Criteria

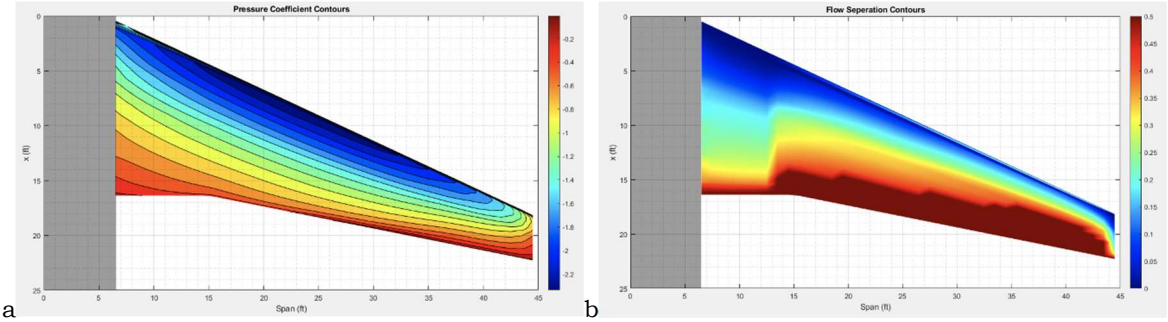

a b

FIGURE 42: Flow Separation Contour for NACA 4412 25˚ Swept Twisted Wing TR=0.25 α=15˚ with 10% Chord Slats and Aileron Interrupted Triple Slotted Flaps. a) *Cp* contours, b) Stratford *S* Criteria

VI Summary & Conclusions

Multi-element high-lift devices on commercial transport aircraft are very complex mechanical systems that induce equally complex air flows around them. In this work, these complex mechanical systems where simplified into geometry that could be easily imputed into a classical vortex lattice panel code. We show how this panel-method code, VORLAX, with a coupled Stratford calculator can estimate on 2D airfoils as well as on 3D wings, regions where flow separation occurs.

Our initial studies of 2D flapped airfoils show that trailing edge devices are capable of greatly increasing the lift coefficient of a wing. Whereas leading edge devices provided marginal increase in lift coefficient, but they provide "relief" to the flow over a wing which keeps it attached to higher angles of attack. By adding both devices at the same time, we can greatly increase the usable maximum lift coefficient of a section.

Three-dimensionality effects are very important in aerodynamics, and thus numerous studies in three-dimensional flow were performed. These studies showed how different parameters are capable of completely changing the flow over the main wing. Common features on transport aircraft such as sweep, taper ratio, or the addition of a Yehudi tend to cause early flow separation to occur on the outboard section of the wing. We reveal that while these inherent tendencies need to be compensated by other features in the deployed "high-lift-system," non-continuous flaps systems - interrupted by design or by failure of a single part to deploy, due to failure - cause an increase in flow separation on the flow ahead of it.

Ultimately, the coupled method used throughout this study is capable of quickly providing insight on preliminary designs of high lift systems and wing planforms. As shown throughout this study, it can be used to run detailed trade studies to identify specific trends associated with design variables.

Acknowledgments

This manuscript derives from work that Mr. Martinez-Rodriguez performed in partial fulfillment of the degree requirements for obtaining his M.S.-degree in Aerospace Engineering from Arizona State University. All design analysis on this unfunded project was completed at Arizona State University.

References

[1] Aeronautical Research Council, "Experiments on an Aerofoil Having a Hinged Rear Portion" R&M 110, 1914.
[2] Smith, A. M. O., "High-lift Aerodynamics," J. Aircraft, Vol. 12, No. 6, pp. 501, 1975.
[3] Page, F.H., "The Handley Page Wing," The Aeronautical Journal, 1921.
[4] Fowler, H.D., "Variable Lift," Western Flying, 1931.
[5] Prandtl, L., "Uber Fltissigkeitsbewegungieb sehr kleiner Reibung," III International Mathematiker-Kongress, Heidelberg, 1904.
[6] White, F., Fluid Mechanics, 8th Edition, McGraw-Hill, 2015.
[7] Küchemann, D., The Aerodynamic Design of Aircraft, AIAA, Virginia, 2012
[8] Stratford, B.S., "The Prediction of Separation of the Turbulent Boundary Layer," Journal of Fluid Mechanics, 1959.
[9] Cebeci, T. & Smith, A.M.O., Analysis of Turbulent Boundary Layers, Academic Press, New York, 1974.
[10] Presz, W.M. & E. T. Pitkins, E.T., "Analytical Model of Axisymmetric Afterbody Flow Separation," AIAA Paper No. 75-65 , 1975.
[11] Miranda, L. R., Baker, R. D., & Elliott, W. M., "A Generalized Vortex-Lattice Method for Subsonic and Supersonic Flow," NASA CR 2875, 1977.
[12] Souders, T.J. & Takahashi, T.T., "VORLAX 2020: Making a Potential Flow Solver Great Again," AIAA 2021-2458, 2021.
[13] Souders, T.J. & Takahashi, T.T., "VORLAX 2020: Benchmarking Examples of a Modernized Potential Flow Solver," AIAA 2021-2459, 2021.
[14] Seetharam, H.C. & Rodgers, E.J., "Experimental Studies of Flow Separation of the NACA 2412 Airfoil," NASA CR 197497 , 1997.
[15] Cebici, T., Mosinskis, G.J. & Smith, A.M.O., "Calculation of Viscous Drag and Turbulent Boundary Layer Separation on Two-Dimensional and Axisymmetric Bodies in Incompressible Flow," MDC J0973-01, McDonnell-Douglas Contractor Report for the Naval Ship Systems Command, 1970. (see https://apps.dtic.mil/sti/pdfs/AD0720775.pdf)
[16] Abbott, I., Von Doenhoff, A. & Stivers, L., "Summary of Airfoil Data," NACA Report 824, National Advisory Committee for Aeronautics, 1945.
[17] Obert, E., Aerodynamic Design of Transport Aircraft, IOS Press, Delft, 2009.
[18] Takahashi, T.T., Aircraft Performance and Sizing, Vol. II: Applied Aerodynamic Design, Momentum Press, 2016.
[19] Pearcey, H.H. & Osborne, J., "Some Problems and Features of Transonic Aerodynamics," ICAS Paper 70-14, International Council of the Aeronautical Sciences, 1970.
[20] Jensen, J. & Takahashi, T.T., "Wing Design Challenges Explained: A Study of the Finite Wing Effects of Camber, Thickness, and Twist," AIAA 2016-0718, 2016.
[21] Takahashi, T.T., Aircraft Performance and Sizing, Vol. I: Fundamentals of Aircraft Performance, Momentum Press, 2016.